

Solution NMR Measurement of Amide Proton Chemical Shift Anisotropy in ^{15}N -Enriched Proteins. Correlation with Hydrogen Bond Length[§]

Nico Tjandra[†] and Ad Bax^{*‡}

Contribution from the Laboratory of Biophysical Chemistry, National Heart, Lung, and Blood Institute, and Laboratory of Chemical Physics, National Institute of Diabetes and Digestive and Kidney Diseases, National Institutes of Health, Bethesda, Maryland 20892-0520

Received March 19, 1997. Revised Manuscript Received May 29, 1997[⊗]

Abstract: Cross-correlation between ^{15}N – ^1H dipolar interactions and ^1H chemical shift anisotropy (CSA) gives rise to different relaxation rates of the doublet components of ^1H – $\{^{15}\text{N}\}$ peptide backbone amides. Two schemes for quantitative measurement of this effect are described and demonstrated for samples of uniformly ^{15}N -enriched ubiquitin and perdeuterated ^{15}N -enriched HIV-1 protease. The degree of relaxation interference correlates with the isotropic ^1H chemical shift, and results indicate that an upfield change of the most shielded principal components of the CSA tensor is correlated with an approximately 2-fold larger downfield shift of the average of the other two components. The magnitude of the relaxation interference is large in β -sheet and considerably smaller in α -helices. This correlation is not dominated by the backbone geometry but reflects the slightly longer hydrogen bond length in helices compared to β -sheet. The smallest relaxation interference effect in ubiquitin is observed for Ser²⁰-H^N and Ile³⁶-H^N, which are the only two amide protons that are not hydrogen bonded in the crystal structure of ubiquitin, inaccessible to solvent, and not highly mobile.

There has been extensive interest in developing a quantitative understanding of the relation between protein structure and chemical shifts.^{1–8} Most work so far has focused on ^{13}C and ^{15}N , and empirical correlations between protein structure and isotropic $^{13}\text{C}^\alpha$ and $^{13}\text{C}^\beta$ chemical shifts have been confirmed by *ab initio* calculations.^{3,9} H ^{α} chemical shifts empirically were also found to be quite sensitive to secondary structure.^{6–8,10–13} As was the case for $^{13}\text{C}^\alpha$ shifts, this dependence primarily results from the chemical shift dependence on the ϕ and ψ backbone torsion angles⁶ and not from hydrogen bonding itself. In contrast, it is well established that the isotropic amide proton chemical shift is strongly influenced by hydrogen bonding.^{13–16}

Measurement of the relatively small ^1H chemical shift anisotropy (CSA) in the solid state is technically challenging, and only a very modest library of ^1H CSA values has been accumulated.¹⁸ For protons involved in a hydrogen bond, these data indicate that the downfield change in isotropic shift associated with increasing hydrogen bond strength is accompanied by an increase in ^1H CSA.¹⁸

In peptidic systems, only three studies on amide proton (H^N) CSA have been published: Reimer and Vaughan reported data for acetanilide,¹⁹ using multipulse ^1H NMR. Opella and co-workers reported CSA values from single crystal ^2H NMR of *N*-acetyl-D,L-valine,²⁰ and, more recently, this group used a three-dimensional solid state NMR experiment to obtain the Leu-H^N shielding tensor in Ala-[^{15}N]Leu.²¹ These data indicate that, although the H^N CSA tensor can deviate from axial symmetry, its most shielded tensor component (σ_{33}) is roughly collinear with the N–H bond.

In this study, we show that quantitative information on the CSA tensor of individual amide protons in ^{15}N -enriched proteins can be readily obtained from measurement of relaxation interference between the $^1\text{H}^\text{N}$ CSA and the $^1\text{H}^\text{N}$ – ^{15}N dipolar relaxation mechanisms. Relaxation of peptide $^1\text{H}^\text{N}$ spins in ^{15}N -enriched proteins is dominated by ^1H – ^1H dipolar interactions, ^1H – ^{15}N dipolar coupling, and $^1\text{H}^\text{N}$ CSA. Assuming, for convenience, that the $^1\text{H}^\text{N}$ CSA tensor is axially symmetric, with

* Corresponding author: Ad Bax, Building 5, Room 126, NIH, Bethesda, MD 20892-0520.

[†] Laboratory of Biophysical Chemistry.

[‡] Laboratory of Chemical Physics.

[§] Keywords: chemical shift anisotropy, cross correlation, dynamics, relaxation, ubiquitin, ^{15}N NMR.

[⊗] Abstract published in *Advance ACS Abstracts*, August 1, 1997.

(1) Ando, I.; Saito, H.; Tabeta, R.; Shoji, A.; Ozaki, T. *Macromolecules* **1984**, *17*, 457–461.

(2) Saito, H. *Magn. Reson. Chem.* **1986**, *24*, 835–852.

(3) de Dios, A. C.; Pearson, J. G.; Oldfield, E. *Science* **1993**, *260*, 1491–1496.

(4) Pearson, J. G.; Oldfield, E.; Lee, F. S.; Warshel, A. *J. Am. Chem. Soc.* **1993**, *115*, 6851–6862.

(5) Oldfield, E. *J. Biomol. NMR* **1995**, *5*, 217–225.

(6) Ósapay, K.; Case, D. A. *J. Am. Chem. Soc.* **1991**, *113*, 9436–9444.

(7) Asakura, T.; Taoka, K.; Demura, M.; Williamson, M. P. *J. Biomol. NMR* **1995**, *6*, 227–236.

(8) Szilagy, L. *Prog. Nucl. Magn. Reson. Spectrosc.* **1995**, *27*, 325–443.

(9) Laws, D. D.; de Dios, A. C.; Oldfield, E. *J. Biomol. NMR* **1993**, *3*, 607–612.

(10) Clayden, N. J.; Williams, R. J. P. *J. Magn. Reson.* **1982**, *49*, 383–396.

(11) Gross, K.-H.; Kalbitzer, H. R. *J. Magn. Reson.* **1988**, *76*, 87–99.

(12) Szilagy, L.; Jardetzky, O. *J. Magn. Reson.* **1989**, *83*, 441–449.

(13) Wishart, D. S.; Sykes, B. D.; Richards, F. M. *J. Mol. Biol.* **1991**, *222*, 541–546.

(14) Pardi, A.; Wagner, G.; Wüthrich, K. *Eur. J. Biochem.* **1983**, *137*, 445–454.

(15) Wagner, G.; Pardi, A.; Wüthrich, K. *J. Am. Chem. Soc.* **1983**, *105*, 5948–5949.

(16) Kuntz, I. D.; Kosen, P. A.; Craig, E. C. *J. Am. Chem. Soc.* **1991**, *113*, 1406–1408.

(17) Duncan, T. M. *A compilation of chemical shift anisotropies*, Farragut Press: Chicago, 1990.

(18) Berglund, B.; Vaughan, R. W. *J. Chem. Phys.* **1980**, *73*, 2037–2043.

(19) Reimer, J. A.; Vaughan, R. W. *J. Magn. Reson.* **1980**, *41*, 483–491.

(20) Gerald II, R.; Bernhard, T.; Haeberlen, U.; Rendell, J.; Opella, S. *J. Am. Chem. Soc.* **1993**, *115*, 777–782.

(21) Wu, C. H.; Ramamoorthy, A.; Gierasch, L. M.; Opella, S. J. *J. Am. Chem. Soc.* **1995**, *117*, 6148–6149.

its most shielded axis parallel to the ¹H–¹⁵N bond, the local field experienced by a ¹H^N attached to ¹⁵N in the |α> spin state corresponds to the sum of the dipolar and CSA tensors; the difference of the dipolar and CSA tensors applies for ¹H^N nuclei attached to a ¹⁵N in the |β> spin state, and the two ¹H^N–{¹⁵N} doublet components therefore relax at different rates. This differential relaxation is commonly referred to as a cross-correlation or relaxation interference effect,^{22–31} and a simple description, directly applicable to the case of peptide ¹H^N–{¹⁵N} groups, has been presented by Goldman.²⁵ In a recent study we demonstrated that peptide ¹⁵N CSA values derived from relaxation interference measurements are in good agreement with solid state NMR measurements.³¹

Here, we describe two slightly different experimental approaches for quantitative measurement of relaxation interference between ¹H^N–¹⁵N dipolar coupling and ¹H^N CSA. Experiments are applied to two ¹⁵N-enriched proteins, ubiquitin (8.6 kD) and perdeuterated HIV-1 protease (a 23 kD homodimer). Results indicate that ¹H^N CSA values indeed correlate with the crystallographically determined hydrogen bond lengths^{32,44} and, as expected, also strongly correlate with the isotropic H^N shift. Remarkably, an increase in shielding in the H–N direction (σ₃₃) is shown to correlate with an approximately equal decrease in (σ₁₁ + σ₂₂)/2. Hence, changes in the principal components of the shielding tensor are highly correlated. Variations in the CSA are therefore much larger than those of the isotropic shifts. H^N CSA values observed in the present study range from a few ppm for buried non-hydrogen bonded amide protons to ca. 14 ppm for short intramolecular hydrogen bonds.

Results and Discussion

Assuming an axially symmetric ¹H^N chemical shift tensor with an angle θ between the orientation of its unique axis and the N–H bond vector, the ¹H^N transverse relaxation rates for the two doublet components of a ¹H^N–¹⁵N spin pair are given by^{25–28}

$$R_2 = \Delta + \lambda \pm \eta \quad (1a)$$

where the + sign applies to the upfield ¹H^N–{¹⁵N} doublet component (¹J_{NH} < 0). Δ, λ, and η correspond to homonuclear dipolar relaxation, ¹H^N–{¹⁵N} dipolar relaxation, and the cross correlation between the ¹H CSA and the ¹H^N–{¹⁵N} dipolar interaction, respectively. They are given by

$$\Delta = q[5J(0) + 9J(\omega_H) + 6J(2\omega_H)] \quad (1b)$$

$$\lambda = d[4J^{dd}(0) + 4\alpha^2 J^{cc}(0) + 3J^{dd}(\omega_H) + 3\alpha^2 J^{cc}(\omega_H) + J^{dd}(\omega_H - \omega_N) + 3J^{dd}(\omega_N) + 6J^{dd}(\omega_H + \omega_N)] \quad (1c)$$

$$\eta = 2\alpha d\{4J^{cd}(0) + 3J^{cd}(\omega_H)\} \quad (1d)$$

where $q = \sum_k \gamma_H^4 h^2 / (80\pi^2 r_{HK}^6)$ and the summation extends over all protons *k* in the vicinity of the amide proton of interest with *r*_{HK} being the interproton distance; $d = \gamma_H^2 \gamma_N^2 h^2 / (80\pi^2 r_{HN}^6)$, $\alpha = -4\pi B_0(\sigma_{||} - \sigma_{\perp})r_{HN}^3 / (3h\gamma_N)$, and *r*_{NH} is the ¹⁵N–¹H internuclear distance, assumed to be 1.02 Å. Relaxation interference between the various ¹H–¹H dipolar terms or between the ¹H–¹H dipolar and ¹H^N–{¹⁵N} dipolar or ¹H^N CSA terms do not need to be considered as it does not affect the initial decay rate of ¹H^N–{¹⁵N} doublet components (although it does result in multiexponential decay of these components). *J*^{dd}(ω), *J*^{cc}(ω), and *J*^{cd}(ω) are the spectral densities for dipolar autocorrelation, CSA autocorrelation, and dipolar-CSA cross correlation, respectively, as defined previously.³¹ For the present case, where θ is assumed to be small (θ ≪ 1) and the relative orientation of the dipolar and CSA tensors is assumed to be independent of internal motion, one has *J*^{dd}(ω) = *J*^{cc}(ω) = *J*^{cd}(ω)/*P*₂(cos θ).³¹ Thus, the superscripts in the spectral density function may be dropped, and eq 1d can be rewritten as

$$\eta = 2\alpha d\{4J(0) + 3J(\omega_H)\}P_2(\cos \theta) \quad (2)$$

In the absence of slow conformational exchange contributions, values for *J*(0) and *J*(ω_H) can be obtained directly from the ¹⁵N *T*₁, *T*₂ and ¹⁵N–{¹H} NOE values by using reduced spectral density mapping:^{33–35}

$$J(\omega_H) = 1/5(\text{NOE} - 1)(\gamma_N/\gamma_H)/(dT_1) \quad (3a)$$

$$J(0) = [1/(dT_2) - 10J(\omega_H) - 3(1 + \alpha^2)J(\omega_N)]/(1 + \alpha^2) \quad (3b)$$

with

$$J(\omega_N) = 1/6[1/(dT_1) - 14J(\omega_H)]/(1 + \alpha^2) \quad (3c)$$

Residues for which conformational exchange contributes to *J*(0) must be excluded when using this procedure. They are readily identified from the *T*₁ and *T*₂ values (using eq 4 of Tjandra et al.³⁷) or from the anomalous decrease in ¹⁵N *T*₂ with increasing magnetic field strength.^{38,39}

Above, the simplifying assumption of an axially symmetric chemical shift tensor was made. This assumption does not limit the general applicability of such a description, as any nonaxially-symmetric tensor can always be decomposed into the sum of two orthogonal axially symmetric shielding tensors. The analysis of relaxation interference for that case is fully analogous to the description given above.²⁵ For the case where one of the principal axes, say σ₃₃, coincides with the N–H bond vector, the asymmetry of the shielding tensor does not affect the cross correlation effect, which in this case is only determined by σ₃₃ – (σ₁₁ + σ₂₂)/2, and not by σ₁₁ – σ₂₂.

(35) Ishima, R.; Nagayama, K. *J. Magn. Reson. B* **1995**, *108*, 73–76.

(36) Farrow, N. A.; Zhang, O.; Szabo, A.; Torchia, D. A.; Kay, L. E. *J. Biomol. NMR* **1995**, *6*, 153–162.

(37) Tjandra, N.; Wingfield, P.; Stahl, S.; Bax, A. *J. Biomol. NMR* **1996**, *8*, 273–284.

(38) Peng, J. W.; Wagner, G. *Biochemistry* **1995**, *34*, 16733–16752.

(39) Phan, I.; Boyd, J.; Campbell, I. D. *J. Biomol. NMR* **1996**, *8*, 369–378.

(22) McConnell, H. M. *J. Chem. Phys.* **1956**, *25*, 709–711.

(23) Mackor, E. L.; MacLean, C. *Progr. Nucl. Magn. Reson. Spectrosc.* **1967**, *3*, 129.

(24) Gueron, M.; Leroy, J. L.; Griffey, R. H. *J. Am. Chem. Soc.* **1983**, *105*, 7262–7266.

(25) Goldman, M. *J. Magn. Reson.* **1984**, *60*, 437–452.

(26) Wimperis, S.; Bodenhausen, G. *Mol. Phys.* **1989**, *66*, 897–919.

(27) Elbayed, K.; Canet, D. *Mol. Phys.* **1989**, *68*, 1033–1046.

(28) Werbelow, L. G. *Encyclopedia of Nuclear Magnetic Resonance*; Grant, D. M., Harris, R. K., Editors-in-Chief; Wiley: London, 1996; Vol. 6, pp 4072–4078.

(29) Dalvit, C. *J. Magn. Reson.* **1992**, *97*, 645–650.

(30) Tolman, J. R.; Prestegard, J. H. *J. Magn. Reson. B* **1995**, *106*, 97–100.

(31) Tjandra, N.; Szabo, A.; Bax, A. *J. Am. Chem. Soc.* **1996**, *118*, 6986–6991.

(32) Vijay-Kumar, S.; Bugg, C. E.; Cook, W. J. *J. Mol. Biol.* **1987**, *194*, 531–544.

(33) Peng, J. W.; Wagner, G. *J. Magn. Reson.* **1992**, *98*, 308–332.

(34) Farrow, N. A.; Zhang, O.; Forman-Kay, J. D.; Kay, L. E. *Biochemistry* **1995**, *34*, 868–878.

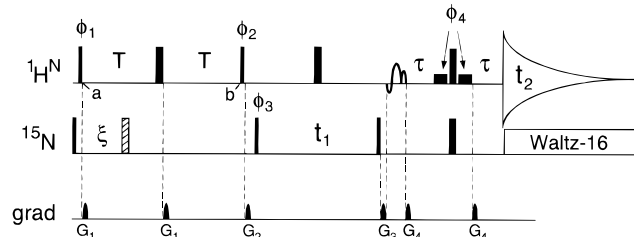


Figure 1. 2D NMR pulse scheme for quantitative measurement of cross-correlation between H^{N} CSA and $\text{H}^{\text{N}}\text{-}^{15}\text{N}$ dipolar coupling. The experiment is carried out twice, once without the shaded ^{15}N 180° pulse (**A**) and once with this 180° pulse included (**B**). All resonances observed with scheme **A** are the result of cross correlation effects during the period $2T$; signals observed in scheme **B** result from regular, INEPT-type magnetization transfer. Narrow and wide pulses correspond to flip angles of 90° and 180° , respectively. The two low power pulses immediately preceding and following the last nonselective ^1H 180° pulse have a width of 1 ms each and correspond to flip angles of 90° . With the carrier positioned on the H_2O resonance, they are part of the WATERGATE water suppression scheme.⁵³ The shaped pulse preceding this WATERGATE pulse combination is of the EBURP type,⁵⁴ with its excitation profile centered at 7.8 ppm and a width of 2.43 ms at 600 MHz ^1H frequency. The radiofrequency phase of all pulses is x , unless indicated. Delay durations: $\tau \approx 1.4$ ms; $\xi = 2.67$ ms, $3.3 \leq T \leq 15$ ms. Phase cycling: $\phi_1 = -x,x$; $\phi_2 = x,x,-x,-x$ (scheme **A**); $\phi_2 = y,y,-y,-y$ (scheme **B**); $\phi_3 = 4(x)$; $4(-x)$; $\phi_4 = -x$; Rec. = x , $2(-x),x$, $-x,2(x),-x$. Quadrature detection in the t_1 dimension is accomplished by incrementing ϕ_3 in the States-TPPI manner. All gradients are sine-bell shaped, with an amplitude of 25 G/cm at their center. Durations: $G_{1,2,3,4} = 1.5, 1, 2, 0.4$ ms, with respective gradient axes: y, x, z, xyz .

For two hydrogen-bonded amides, Opella and co-workers found that the most shielded axis of the H^{N} CSA tensor deviates by less than 10° from the N–H bond vector, and $|\sigma_{22} - \sigma_{11}| \ll |\sigma_{33} - (\sigma_{11} + \sigma_{22})/2|$.^{20,21} This strongly suggests that, at least for hydrogen bonded amides, the approximation of an axially symmetric H^{N} CSA tensor, aligned with the N–H bond, is reasonable. Calculation of the $^1\text{H}^{\text{N}}$ CSA from the magnitude of the relaxation interference effect is based on the assumption that the $^1\text{H}^{\text{N}}\text{-}^{15}\text{N}$ dipolar coupling is a constant, and all variations in αd (eq 1d) are attributed to changes in the chemical shift tensor.

Measurement Schemes. We present two different methods for measuring the relaxation interference: one 2D experiment which is a simple modification of the commonly used $^1\text{H}\text{-}^{15}\text{N}$ HSQC experiment and a 3D experiment which measures the relative amplitude of the $^1\text{H}^{\text{N}}$ doublet components after a constant-time evolution period. The first approach conceptually is analogous to the method previously described for measurement of ^{15}N CSA values;³¹ the second one is quite general and provides a sensitive and robust method for measuring cross correlation for many different types of interactions.

CSA from 2D $^1\text{H}\text{-}^{15}\text{N}$ Correlation. Figure 1 shows the 2D pulse scheme used for quantitative measurement of relaxation interference between the $^1\text{H}^{\text{N}}$ CSA and $^1\text{H}\text{-}^{15}\text{N}$ dipolar coupling mechanisms. The pulse scheme is similar to the regular $^1\text{H}\text{-}^{15}\text{N}$ HSQC correlation experiment⁴⁰ in which the first INEPT transfer from ^1H to ^{15}N is modified.²⁹ The experiment is performed twice: once without applying the shaded 180° ^{15}N pulse and once with application of this pulse. In the following these experiments will be referred to as **A** and **B**, respectively. Intensity observed in spectrum **A** will be shown to result exclusively from relaxation interference, whereas

spectrum **B** yields a reference spectrum where magnetization transfer occurs in the regular manner, through J_{NH} coupling.

In scheme **A**, $^1\text{H}^{\text{N}}$ magnetization (represented by I) precesses in the transverse plane between time points *a* and *b*, for a period $2T$. In the absence of the 180° ^{15}N pulse, effects of both $^1\text{H}^{\text{N}}$ chemical shift and J_{NH} coupling are refocused at time *b*. Thus, at time point *b* the transverse magnetization of the two $^1\text{H}^{\text{N}}\text{-}\{^{15}\text{N}\}$ doublet components, both aligned along the $-y$ axis, are described by $-I_y/2 \pm I_y S_z$. The upfield doublet component, $I_y S_z - I_y/2$, relaxes at a rate $\Delta + \lambda - \eta$, whereas the downfield component relaxes at $\Delta + \lambda + \eta$ (cf. eq 1). Calculations indicate that transverse cross relaxation between the two doublet components,²⁵ which precess at different frequencies, may be safely ignored. Thus, for scheme **A**, the transverse magnetization at time point *b* in Figure 1 is given by

$$\sigma_b^{\text{A}} = (I_y S_z - I_y/2) \exp[-2T(\Delta + \lambda - \eta)] + (-I_y S_z - I_y/2) \exp[-2T(\Delta + \lambda + \eta)] = I_y S_z (\epsilon^- - \epsilon^+) - I_y (\epsilon^+ + \epsilon^-)/2 \quad (4)$$

where $\epsilon^\pm = \exp[-2T(\Delta + \lambda \pm \eta)]$. The antiphase term, $I_y S_z (\epsilon^- - \epsilon^+)$, is transferred into antiphase ^{15}N magnetization at time *b* and gives rise to a regular HSQC spectrum in which resonance amplitudes are proportionate to $\epsilon^- - \epsilon^+$.

For scheme **B**, the 180° ^{15}N pulse applied at time $\xi = 1/(4J_{\text{NH}})$ after the initial 90° ^1H pulse causes the two doublet components to be aligned along the $\pm x$ axis at time point *b*, yielding

$$\sigma_b^{\text{B}} = (I_x/2 - I_x S_z) \exp[-2T(\Delta + \lambda - \eta) + 2\xi\eta] - (I_x/2 + I_x S_z) \exp[-2T(\Delta + \lambda + \eta) - 2\xi\eta] \quad (5a)$$

In practice, $2\xi\eta \ll 1$, and

$$\begin{aligned} \exp[-2T(\Delta + \lambda - \eta) + 2\xi\eta] + \exp[-2T(\Delta + \lambda + \eta) - 2\xi\eta] &\approx \\ \exp[-2T(\Delta + \lambda - \eta)] + \exp[-2T(\Delta + \lambda + \eta)] &= \epsilon^- + \epsilon^+ \end{aligned} \quad (5b)$$

Fully analogous to scheme **A**, the antiphase term present at time point *b*, $I_x S_z (\epsilon^- + \epsilon^+)$, is transferred into antiphase ^{15}N magnetization and gives rise to a HSQC spectrum in which resonance amplitudes are proportionate to $\epsilon^- + \epsilon^+$. Thus, the ratio of the signal intensities obtained with schemes **A** and **B** equals

$$I_{\text{A}}/I_{\text{B}} = (\epsilon^- - \epsilon^+) / (\epsilon^- + \epsilon^+) = \tanh(2T\eta) \quad (6)$$

Note that this intensity ratio depends only on η and T and therefore permits η to be extracted straightforwardly. The sensitivity of the experiment is also affected by the homonuclear and heteronuclear dipolar relaxation rates, however. For $\eta \ll \Delta + \lambda$, sensitivity of the experiment is maximum for $2T \approx (\Delta + \lambda)^{-1}$.

CSA from Constant-Time H^{N} Evolution. A second way for observing relaxation interference measures the relative amplitudes of the two doublet components at the end of a constant-time evolution period. This principle is very general and easily applicable to the measurement of numerous other types of relaxation interference too. The pulse scheme used for measuring relaxation interference between H^{N} CSA and $\text{H}^{\text{N}}\text{-}^{15}\text{N}$ dipolar couplings is shown in Figure 2. It is very similar to scheme **A** of Figure 1, but the position of the first 180° ^1H

(40) Bodenhausen, G.; Ruben, D. J. *Chem. Phys. Lett.* **1980**, *69*, 185–189; Bax, A.; Ikura, M.; Kay, L. E.; Torchia, D. A.; Tschudin, R. *J. Magn. Reson.* **1990**, *86*, 304–318.

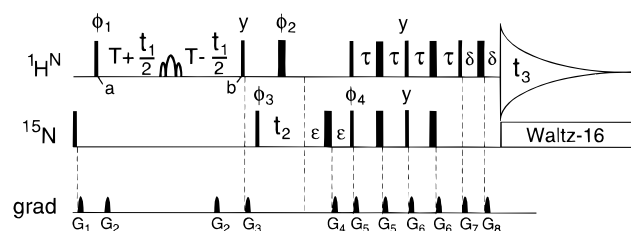


Figure 2. Pulse scheme of the 3D gradient-enhanced HNH experiment for quantitative measurement of cross-correlation between $^1\text{H}^{\text{N}}$ CSA and $^1\text{H}^{\text{N}}-^{15}\text{N}$ dipolar coupling. Narrow and wide pulses correspond to flip angles of 90° and 180° , respectively. The shaped 180° ^1H pulse, applied during the constant-time t_1 evolution period is of the V1 type,⁴³ with a total duration of 3.7 ms for an inversion profile width of 2.2 kHz. The ^1H carrier is positioned in the center of the amide region. Phase cycling: $\phi_1 = x$; $\phi_2 = 2(x), 2(y), 2(-x), 2(-y)$; $\phi_3 = x, -x$; $\phi_4 = x$; Rec. = $x, -x$. Quadrature detection in the t_1 dimension is obtained by incrementing ϕ_1 in the States-TPPI manner.⁵⁵ Quadrature detection in the t_2 dimension is obtained by inverting the polarity of G_4 together with ϕ_4 , with data stored separately, in order to obtain Rance-Kay style data.⁵⁶ Delay durations: $\epsilon = 3.4$ ms, $\tau = 2.67$ ms; $\delta = 1.2$ ms. All gradients are sine-bell shaped, with an amplitude of 25 G/cm at their center. Gradient durations: $G_{1,2,3,4,5,6,7,8} = 2.5, 1.1, 1.3, 2.72, 0.8, 1.3, 0.2, 0.075$ ms; the respective gradient axes are xy, y, xz, z, x, y, z, z .

pulse is shifted in a constant-time manner,^{41,42} and data in this case are recorded most conveniently as a 3D spectrum, with the ^{15}N -coupled $^1\text{H}^{\text{N}}$ in the F_1 dimension, ^{15}N in F_2 , and ^{15}N -decoupled $^1\text{H}^{\text{N}}$ in F_3 . Although at first sight it may appear inefficient to have the $^1\text{H}^{\text{N}}$ resonance in both the F_1 and F_3 dimension of the spectrum, this is offset by the simplicity of the experiment and the unambiguous nature of the results. Moreover, a narrow spectral width may be used in the F_1 dimension because the resulting aliasing will never give rise to resonance overlap, provided the spectral width is larger than the $^1J_{\text{NH}}$ splitting.

Analogous to the above description of the 2D cross correlation experiment, the two $^1\text{H}^{\text{N}}$ doublet components at time point a in Figure 2 are described by $-I_y/2 \pm I_y S_z$. The density operator for the downfield doublet component at time a is given by $\sigma_a^\alpha = -I_y/2 - I_y S_z$. After evolution during the constant time period and relaxation for a duration $2T$, it is given by

$$\sigma_b^\alpha(t_1) = -(S_z + 1/2)\{I_y \cos[2\pi(\delta - J_{\text{NH}}/2)t_1] + I_x \sin[2\pi(\delta - J_{\text{NH}}/2)t_1]\} \exp[-2T(\Delta + \lambda - \eta)] \quad (7a)$$

Similarly, the upfield component is described by

$$\sigma_b^\beta(t_1) = (S_z - 1/2)\{I_y \cos[2\pi(\delta + J_{\text{NH}}/2)t_1] + I_x \sin[2\pi(\delta + J_{\text{NH}}/2)t_1]\} \exp[-2T(\Delta + \lambda + \eta)] \quad (7b)$$

The $I_y S_z$ terms in eqs 7a and 7b are transformed into transverse ^{15}N magnetization by the 90° $^1\text{H}/^{15}\text{N}$ pulse pair applied at time b . Following ^{15}N evolution during t_2 , the $^1\text{H}^{\text{N}}$ signal is observed during t_3 . Thus, after 3D Fourier transformation each amide yields two resonances in the F_1 dimension, at frequencies $\delta \pm J_{\text{NH}}/2$, and with an amplitude ratio

$$I^\alpha/I^\beta = -\exp(4T\eta) \quad (8)$$

Extracting η from eq 8 at high precision requires the two doublet components to be well-resolved, mandating the use of relatively long values of $2T$. A H^{N} band-selective refocusing pulse is used in this constant-time evolution period in order to

(41) Bax, A.; Mehlkopf, A. F.; Smidt, J. *J. Magn. Reson.* **1979**, *35*, 167–169.

(42) Sørensen, O. W. *J. Magn. Reson.* **1990**, *96*, 433–438.

reduce losses resulting from homonuclear $J_{\text{HNH}\alpha}$ dephasing. It is critical that the amplitude profile of this pulse is sufficiently flat, such that it does not affect the relative intensities of the two doublet components which are displaced by $^1J_{\text{NH}}$ in the ^1H dimension. The V1 pulse of Abramovich and Vega⁴³ was found suitable for this purpose.

Both the schemes of Figures 1 and 2 have been tested extensively on a sample of ^{15}N -labeled ubiquitin. The scheme of Figure 1 also has been applied to a sample of perdeuterated HIV protease, complexed with the symmetric inhibitor DMP-323.⁴⁴ Possible complications resulting from homonuclear $\text{H}^{\text{N}}-\text{H}^\alpha$ J coupling or other homonuclear relaxation interference effects are minimized in such a perdeuterated sample. These results therefore serve as an experimental check on the possible influence of such effects.

A detailed attempt to correlate the CSA values with molecular structure has been carried out only for ubiquitin, for which a higher resolution crystal structure is available. HIV protease CSA values (Supporting Information) qualitatively agree well with observations listed below for ubiquitin. However, quantitative analysis is complicated by the lower resolution of this structure compared to ubiquitin and by the fact that in the protease crystal structure the two monomers of this homodimeric protein differ substantially in structure, whereas only a single set of NMR resonances is observed. In solution, this asymmetry presumably is also present on a sub-microsecond time scale, but rapid averaging between the different conformations results in a single set of resonances.⁴⁵

$^1\text{H}^{\text{N}}$ CSA Values in Ubiquitin. The schemes of Figures 1 and 2 have been applied to a sample of uniformly ^{15}N -enriched human ubiquitin. Figure 3A shows a small section of the 2D spectrum recorded with Figure 1, scheme A, i.e., with all observed intensity resulting from cross correlation. A total dephasing time, $2T$, of 22 ms was used, and the sample temperature was set to 13.6 °C. At this temperature, the effective rotational correlation time derived from ^{15}N T_1 and T_2 values, $\tau_c = 1/(2 \text{Tr } \mathbf{D})$, equals 6.02 ns, and the rotational diffusion tensor, \mathbf{D} , was found to be axially symmetric, with the same orientation of the symmetry axis and $D_{\parallel}/D_{\perp} = 1.17$ as reported previously at higher temperature.⁴⁶ Figure 4 shows the intensity ratio, I_A/I_B , as a function of dephasing time for a number of residues, best fit to eq 6. Values of the $^1\text{H}^{\text{N}}$ CSA were calculated from these data using eqs 2 and 6, and spectral densities of eq 3, assuming that the $^1\text{H}^{\text{N}}$ CSA tensor is axially symmetric with its unique axis collinear with the N–H bond vector ($\theta = 0$).

Figure 3B shows F_1 traces taken from the 3D spectrum, recorded with the pulse scheme of Figure 2, and using a dephasing delay, $2T$, of 40 ms. The variation in the relative intensities of the three amide proton doublets is clearly visible. The experiment has been carried out for three different durations of $2T$: 40, 75, and 110 ms. These three data sets yield remarkably similar values of the $^1\text{H}^{\text{N}}$ CSA (Figure 1, supporting information), although, as expected, a small decrease in the derived CSA values is observed for the longest value of $2T$, where the assumption of monoexponential decay breaks down.

(43) Abramovich, D.; Vega, S. *J. Magn. Reson. A* **1993**, *105*, 30–48. Ogura, K.; Terasawa, H.; Inagaki, F. *J. Magn. Reson. B* **1993**, *112*, 63–68.

(44) Lam, P. Y. S.; Jadhav, P. K.; Eyermann, C. J.; Hodge, C. N.; Ru, Y.; Bacheler, L. T.; Meek, J. L.; Otto, M. J.; Rayner, M. M.; Wong, Y. N.; Chang, C.-H.; Weber, P. C.; Jackson, D. A.; Sharpe, T. R.; Erickson-Viitanen, S. *Science* **1994**, *263*, 380–384.

(45) Nicholson, L. K.; Yamazaki, T.; Torchia, D. A.; Grzesiek, S.; Bax, A.; Stahl, S. J.; Kaufman, J. D.; Wingfield, P. T.; Lam, P. Y. S.; Jadhav, P. K.; Hodge, C. N.; Dommelle, P. J.; Chang, C.-H. *Nature Struct. Biol.* **1995**, *2*, 274–280.

(46) Tjandra, N.; Feller, S. E.; Pastor, R. W.; Bax, A. *J. Am. Chem. Soc.* **1995**, *117*, 12562–12566.

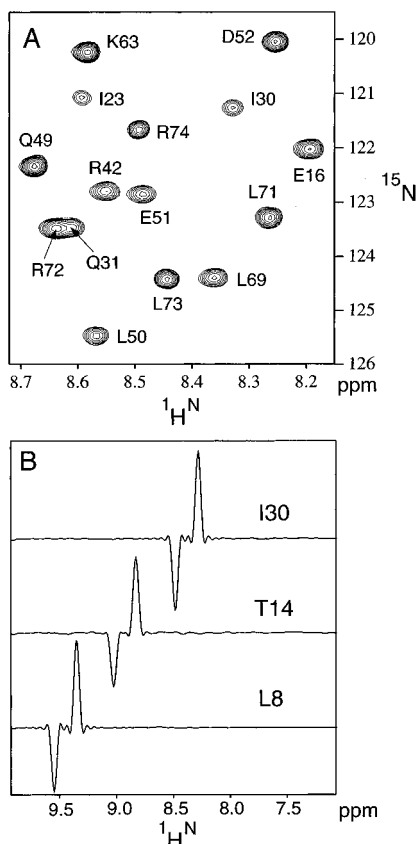


Figure 3. Sections from the 600 MHz ubiquitin spectra from which $^1\text{H}^{\text{N}}$ CSA values were extracted. (A) Small section of the 2D spectrum recorded with scheme A of Figure 1, using a $2T$ duration of 22 ms. (B) F_1 traces taken from the 3D spectrum at the (F_2, F_3) frequencies of Ile³⁰, Thr¹⁴, and Leu⁸. The spectrum was recorded with the scheme of Figure 2, using a $2T$ duration of 40 ms.

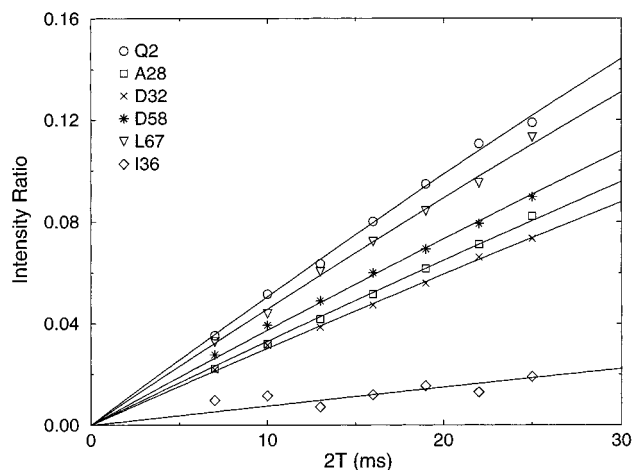


Figure 4. Ratio of the resonance intensities observed with schemes A and B of Figure 1, as a function of the cross-correlation build-up duration, $2T$. Solid lines correspond to the calculated best fit to eq 7.

The pairwise root-mean-square difference (rmsd) between the $^1\text{H}^{\text{N}}$ CSA values extracted from the build-up of the cross correlation effect in the 2D spectra (Figure 4) and from the 3D spectrum equals 1.4 ppm. In all further analysis, we will use the average of these two values, which then includes a random error of 0.7 ppm.

Figure 5 shows the measured $^1\text{H}^{\text{N}}$ CSA values as a function of residue. The data in Figure 5 suggest that CSA values in ubiquitin's five-stranded β -sheet (11.2 ± 1.6 ppm) are significantly larger than those in its α -helix or its short 3_{10} -helix. However, in contrast to what has been observed for isotropic

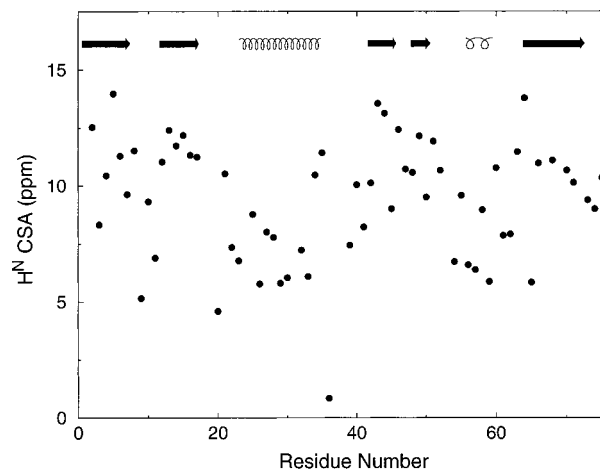


Figure 5. $^1\text{H}^{\text{N}}$ CSA calculated from the quantitative cross-correlation experiments, as a function of residue number. Ubiquitin's secondary structure is marked at the top (solid arrow: β -sheet; small pitch coil: α -helix; large pitch coil: 3_{10} helix). The CSA tensor is assumed to be axially symmetric, with its unique axis collinear with the N-H bond direction.

$^{13}\text{C}^{\alpha}$ shifts, for example, the correlation between secondary structure and $^1\text{H}^{\text{N}}$ CSA is apparently not dominated by the backbone torsion angles. For example, although α -helical amide protons have small CSA values (7.2 ± 1.5 ppm), Asp⁵², which also has nearly α -helical backbone angles but hydrogen-bonds to solvent, shows a relatively large CSA of 10.7 ppm. Similarly, several residues with β -sheet type backbone angles, but lacking the characteristic hydrogen bonds, have low CSA values (Lys¹¹, Ile³⁶).

$^1\text{H}^{\text{N}}$ CSA and Hydrogen Bond Length. Figure 6 shows the correlation between the measured $^1\text{H}^{\text{N}}$ CSA and hydrogen bond length. As was previously reported for OH \cdots O hydrogen bonds,¹⁸ the $^1\text{H}^{\text{N}}$ proton CSA also depends strongly on the length of the hydrogen bond. The scatter in the correlation of Figure 6 must, in part, result from the considerable uncertainty in the accuracy with which the hydrogen bond length can be determined from a X-ray crystal structure, solved at 1.8 Å resolution. Highly mobile amides, for which the ^{15}N order parameter, S^2 , is smaller than 0.75, have been excluded from this plot as such high degrees of mobility suggest that the crystallographically observed hydrogen bond lengths are not representative for the solution structure.

Hydrogen bonds are electrostatic in nature, and, ignoring electrostatic shielding at the very short distances involved, the electric field at the $^1\text{H}^{\text{N}}$ nucleus from the hydrogen bond accepting oxygen is expected to decrease with the square of the distance between the proton and the position of the negative charge on the oxygen atom. Best agreement between an equation of the type

$$\text{CSA} = B + C/(r_{\text{H}\cdots\text{O}} - D)^2 \quad (9)$$

is obtained for $B = 4.9$ ppm, $C = 1.96$ ppm Å², and $D = 1.3$ Å. Here, B is the $^1\text{H}^{\text{N}}$ CSA value expected in the absence of hydrogen bonding. The rmsd between values predicted by eq 9 and measured CSA values is 1.8 ppm. Ser²⁰-H^N and Ile³⁶-H^N are the only amide hydrogens in ubiquitin that are not hydrogen bonded in the crystal structure and which are not accessible to solvent. With values of 4.6 and 0.9 ppm, respectively, these two amides yielded the lowest CSA values observed in ubiquitin. Similarly, the three amides with the lowest $^1\text{H}^{\text{N}}$ CSA values in HIV-protease (Gln⁷, Met³⁶, Gln⁹², Supporting Information), complexed with the symmetric inhibi-

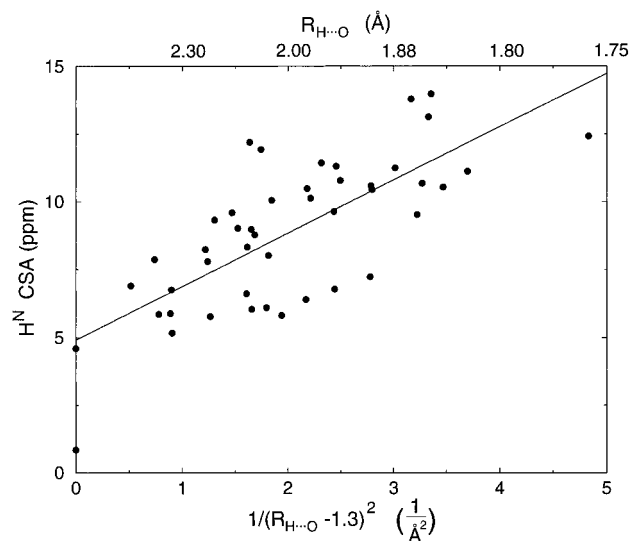


Figure 6. Correlation between H^N CSA and hydrogen bond length in human ubiquitin. Hydrogens were added to the X-ray crystal structure³² with the program X-PLOR.⁵⁷ Amides with low order parameters ($S^2 < 0.75$) and solvent-exposed amides for which no hydrogen bonded water was observed in the crystal structure are not included. The correlation coefficient, r , is 0.735. The solid line corresponds to eq 9, and the statistical significance, p , of this correlation is 10^{-8} . The error estimated in the crystallographically determined hydrogen bond lengths equals 0.15 \AA ; the random error in the CSA measurement equals 0.7 ppm .

tor DMP-323,⁴⁴ are also not hydrogen bonded or solvent-accessible in the crystal structure of this complex.

H^N CSA and Solvent Interaction. Besides Ser²⁰ and Ile³⁶, there are numerous other amide protons in ubiquitin which lack an intramolecular hydrogen bonding partner in the crystal structure, but these amides are all exposed to solvent and presumably are engaged in hydrogen bonding to water oxygens. These solvent exposed amides (marked "S" in Figure 7) have relatively large CSA values of $10.5 \pm 1.6 \text{ ppm}$, i.e., they are only slightly smaller than CSA values observed in β -sheet.

H^N CSA and Isotropic Shift. The isotropic H^N shift has long been recognized as an indicator for hydrogen bond strength.^{13–16} Thus, if the H^N CSA is also representative of hydrogen bond strength, it is expected that the H^N CSA and the H^N isotropic shift are strongly correlated. Indeed, such a correlation is observed (Figure 7). Remarkably, however, an increase in shielding in the direction of the N–H bond vector is accompanied by a decrease in the isotropic shift. A best fit between the CSA and the isotropic chemical shift (δ_i) yields

$$\delta_i = 5.5 - 0.3 (\delta_{\parallel} - \delta_{\perp}) \text{ ppm} \quad (10)$$

where δ_{\perp} and δ_{\parallel} are chemical shifts perpendicular and parallel to the unique axis of the chemical shift tensor which is assumed to be axially symmetric [$\delta_{\perp} = -(\sigma_{11} + \sigma_{22})/2$; $\delta_{\parallel} = -\sigma_{33}$]. With $\delta_i = (\delta_{\parallel} + 2\delta_{\perp})/3$, this indicates that a decrease in δ_i correlates with a 2-fold larger increase in δ_{\perp} .

β -Sheet and α -helical amide protons in Figure 7 are marked "B" and "A", respectively. As can be seen from the figure, amides making α -helical hydrogen bonds tend to have smaller CSA values than β -sheet residues, whereas their isotropic shifts are less clearly distinguished. Glu³⁴- H^N is the only amide making an α -helical $H^N \cdots O'_{i-4}$ hydrogen bond with a large (10.5 ppm) CSA. Although this residue is identified by the MOLMOL program⁴⁷ as the last residue of ubiquitin's α -helix, its backbone angles ($\phi = -124^\circ$; $\psi = -6^\circ$) fall well outside

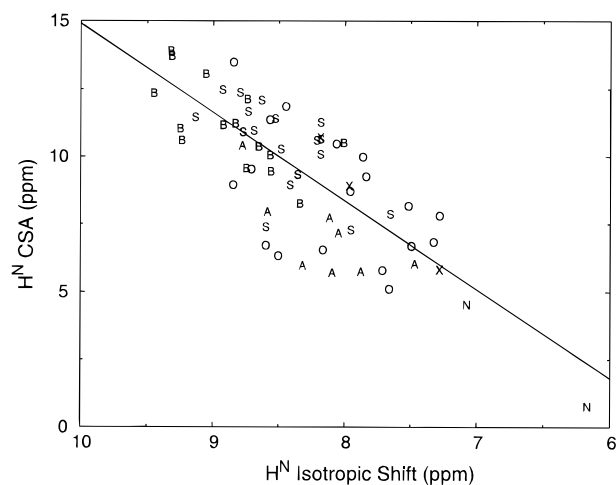


Figure 7. Correlation between isotropic H^N shift and H^N CSA. Amides involved in different types of hydrogen bonding are marked as follows: α -helix: A; β -sheet: B; 3_{10} : X; solvent-exposed or hydrogen bonded to water in X-ray: S; other (backbone–backbone or backbone–side chain): O; not hydrogen bonded: N. The correlation coefficient, r , equals 0.782. The solid line corresponds to eq 10, and the statistical significance, p , of the correlation is $< 10^{-12}$. The random error in the CSA measurement equals 0.7 ppm .

the regular α -helical range and the hydrogen bond length in the crystal structure is shorter than that of other α -helical amides. It is also important to point out that the small CSA values in α -helices are only an indirect consequence of the secondary structure and presumably reflect the fact that α -helical hydrogen bonds typically are slightly longer than those in β -sheet. It is therefore expected that most α -helices will include also some amides with H^N CSA values comparable to those found in β -sheet and *vice versa*.

Concluding Remarks

Our data represent the first extensive measurement of H^N chemical shift anisotropies in polypeptides. These results will be critical for validating *ab initio* proton chemical shift calculations, which hold the key to explaining the exquisite sensitivity of proton chemical shifts to local structure. Once such correlations have been unambiguously established, it may become possible to interpret small changes in either the isotropic chemical shift or the CSA, which occur upon mutation or ligation of a protein, in terms of minute structural rearrangements.

A 2D and a 3D method for quantitative measurement of relaxation interference between the H^N – ^{15}N dipolar coupling and H^N CSA yield good agreement on the magnitude of the H^N CSA. This indicates that this CSA value can be measured reliably either from the relative intensities in a pair of simple 2D H^N – ^{15}N shift correlation spectra or from relative intensities of two doublet components in a constant-time type 3D experiment. This latter method represents a generally applicable new approach for quantitative measurement of relaxation interference between J -coupled nuclei. Preliminary, unpublished results show that it is applicable to measurement of the CSA of $^{13}C^\alpha$ and side-chain carbons, $^{13}C'$, ^{15}N , and also protons other than H^N . Using such experiments, the magnitude of the shielding tensor of a given nucleus can be mapped in many different directions, depending on the pair of nuclei chosen in a given experiment. In favorable cases, determination of the entire shielding tensor, including its orientation in the molecular frame, appears feasible.

The measured H^N CSA values in ubiquitin range from near zero in the absence of hydrogen bonding to *ca.* 14 ppm for

(47) Koradi, R.; Billeter, M.; Wüthrich, K. *J. Mol. Graphics* **1996**, *14*, 52–55.

residues involved in short hydrogen bonds. Solid state NMR has conclusively shown that for near-planar OH...O hydrogen bond arrangements between carboxylates there is a well defined correlation between the proton CSA and the length of the hydrogen bond, with a 2-fold drop in magnitude when the O—O distance increases from 2.4 to 2.75 Å.¹⁸ The dependence of the ¹H^N CSA on hydrogen bond length appears to be similarly steep. Presumably this steeper-than- r^{-2} dependence reflects the fact that the center of the atomic charges does not coincide with the positions of the nuclei. In part, it may also be caused by the increase of the effective dielectric constant with increasing distance, owing to the polarizability of nearby groups.⁴⁸

An increase in hydrogen bond strength increases the shielding parallel to the N—H bond but decreases the shielding orthogonal to this bond. As a consequence, hydrogen bonding has a much larger effect on the CSA than on the isotropic chemical shift. These observations rule out the possibility that the effect of hydrogen bonding on the amide proton chemical shielding tensor is dominated by the anisotropic magnetic susceptibility of the nearby carbonyl group. It remains unclear, however, whether the CSA as measured from relaxation interference is a better measure for hydrogen bond strength than the isotropic H^N shift; the scatter in the correlation of Figure 6 is comparable to what is observed when plotting the isotropic shift *versus* hydrogen bond length.

Solvent-exposed amides show large and relatively uniform CSA values of 10.5 ± 1.6 ppm, and no significant difference is found between amides for which a hydrogen-bonded water molecule is observed in the crystal structure and those for which this is not the case. This suggests that the presence or absence of a hydrogen-bonded water molecule is not related to the hydrogen bond strength but merely reflects the positional uncertainty of such a water molecule in the crystalline state.

Experimental Section

NMR experiments were carried out at 13.6 °C on a sample of commercially obtained (U-¹⁵N)-ubiquitin (VLI Research, Southeastern, PA), 1.4 mM, pH 4.7, 10 mM NaCl and at 27 °C on a sample of ¹⁵N-enriched HIV protease-DMP323 complex^{44,49} (0.75 mM of dimer in a 250 μL Shigemi microcell) in H₂O/D₂O (95%/5%), 50 mM sodium acetate buffer (pH 5.2), with ≥85% deuteration of its nonexchangeable protons. All NMR experiments were carried out using a Bruker DMX-600 NMR spectrometer, operating at a ¹H resonance frequency of 600 MHz. A three-axis pulsed field gradient ¹H/¹⁵N/¹³C probehead, optimized for ¹H detection, was used.

A series of 2D experiments was carried out on ubiquitin at 13.6 °C, using the pulse scheme of Figure 1. Data matrices consisted of 768* (t_1) × 128* (t_2) data points, with acquisition times of 64 ms (t_1) and 83 ms (t_2). A total of 32 scans per complex t_1 increment was collected for scheme **A** (Figure 1), whereas eight scans were accumulated in the reference experiment, **B** (Figure 1). The total measuring time for such a pair of experiments was 5.2 h. Experiments were repeated for the

(48) Sharp, K. A.; Honig, B. *Annu. Rev. Biophys. Biophys. Chem.* **1990**, *19*, 301–332.

(49) Yamazaki, T.; Nicholson, L. K.; Torchia, D. A.; Stahl, S. J.; Kaufman, J. D.; Wingfield, P. T.; Domaille, P. J.; Campbell-Burk, S. *Eur. J. Biochem.* **1994**, *219*, 707–712.

following durations of the dephasing delay, 2T: 7, 10, 13, 16, 19, 22, 25, 28, and 31 ms. All experiments were performed with the ¹H carrier positioned on the H₂O resonance and the ¹⁵N carrier at 116.5 ppm.

H^N CSA values in HIV-protease were derived from a single set of 2D experiments, carried out with a dephasing delay of 22 ms. The data matrix size and number of scans were as listed above, but the total measuring time was 12 h, owing to the longer delay between scans, needed because of the longer T_1 relaxation times of the amide protons. Spectral densities were derived from eq 3, using ¹⁵N T_1 , T_2 , and NOE values reported previously for the same sample, at the same temperature.³⁷

Ubiquitin ¹⁵N T_1 and T_2 measurements were made at 13.6 °C, using the same procedures as were used previously at higher temperature.⁴⁶ The value of $1/(2 \text{ Tr } \mathbf{D})$, corresponding to the rotational correlation time in the case of isotropic tumbling, was derived from these data and determined to be 6.02 ns. The anisotropy and orientation of the diffusion tensor were indistinguishable from values at 27 °C, reported previously.⁴⁶ No ¹⁵N-¹H NOE values were measured at 13.6 °C, and NOE values previously measured at 27 °C were used instead. Note that the resulting small error in $J(\omega_{\text{H}})$ (*cf.* eq 3a) has a negligible effect on the derived CSA because the CSA is dominated by $J(0)$, which is two orders of magnitude larger than $J(\omega_{\text{H}})$.

All data sets were processed using the program NMRPipe⁵⁰ and analyzed with the program PIPP.⁵¹ Resonance intensities were obtained from peak heights using three-data-point interpolation,⁵¹ and resonance assignments are taken from Wang et al.⁵²

Acknowledgment. We thank Marius Clore, James A. Ferretti, Attila Szabo, Dennis Torchia, and Rob Tycko for useful discussions, Paul Wingfield and Steven Stahl for the sample of [²H,¹⁵N]-HIV1-protease, and Chong-Hwan Chang (Dupont-Merck) for providing us with the X-ray coordinates of the DMP323-protease complex. This work was supported by the Intramural AIDS Targeted Anti-Viral Program of the Office of the Director of the National Institutes of Health.

Supporting Information Available: One table with ubiquitin H^N CSA values; one table with H^N CSA values of HIV-protease, complexed with the inhibitor DMP-323; one figure showing the correlation between H^N CSA measured from a 40-ms constant-time 3D HNH experiment with those measured from 75 and 110 ms (5 pages). See any current masthead page for ordering and Internet access instructions.

JA970876E

(50) Delaglio, F.; Grzesiek, S.; Vuister, G. W.; Zhu, G.; Pfeifer, J.; Bax, A. *J. Biomol. NMR* **1995**, *6*, 277–293.

(51) Garrett, D. S.; Powers, R.; Gronenborn, A. M.; Clore, G. M. *J. Magn. Reson.* **1991**, *94*, 214–220.

(52) Wang, A. C.; Grzesiek, S.; Tschudin, R.; Lodi, P. J.; Bax, A. *J. Biomol. NMR* **1995**, *5*, 376–382.

(53) Piotto, M.; Saudek, V.; Sklenar, V. *J. Biomol. NMR* **1992**, *2*, 661–665.

(54) Geen, H.; Freeman, R. *J. Magn. Reson.* **1991**, *93*, 93–141.

(55) Marion, D.; Ikura, M.; Tschudin, R.; Bax, A. *J. Magn. Reson.* **1989**, *85*, 393–399.

(56) Kay, L. E.; Keifer, P.; Saarinen, T. *J. Am. Chem. Soc.* **1992**, *114*, 10663–10665.

(57) Brünger, A. T. *X-PLOR Version 3.1: A System for X-ray Crystallography and NMR*; Yale University Press: New Haven, CT, 1992.